Colloidal metal oxide nanoparticles prepared by laser ablation technique and their antibacterial test

J.S Duque[1*], B. M. Madrigal[2], Y.P. Avila[2], H. Riascos[1]

[1] *Plasma, Laser and Applications Research Group, Basic Science Department, Technological University of Pereira, A.A. 097, Pereira 660003, Colombia.*

[2] *Coordination and Organometallic Applied to Molecular Materials, Chemistry Department, Technological University of Pereira, A.A. 097, Pereira 660003, Colombia.*

*joseduque@utp.edu.co

Abstract

We report the production of metal oxide ($TiFe_2O_4$, $ZnFe_2O_4$) nanoparticles by pulsed laser ablation technique in liquid environment. We used nano second Nd: YAG laser systems working at 532 nm and 1064 nm of wavelength, the energy of the laser beam was kept constant at 80 mJ. Absorbance spectra, surface plasmon resonance, optical band-gap and nanoparticle morphology were investigated using ultraviolet-visible (UV-Vis) spectroscopy, Fourier transform infrared spectroscopy (FTIR), and scanning electron microscopy (SEM). Changing the wavelength of the laser for growth, nanoparticles shown shift between the absorbance and surface plasmon resonance peaks in their UV-Vis spectra, this implies that the optical properties of the colloid nanoparticles depends on laser parameters, this was confirmed with the variation of the band gap energy. Furthermore, red shift for the absorbance peak was observed for samples as-growth at 532 nm around the 150 nm as function of time preparation. Whereas, for the samples as-growth at 1064 nm there is no shift in the absorbance spectra, this can be due to agglomeration and formation of larger particles. The characterization results shown appropriate plasmonic photo-catalysts properties of the particles, hence the photo activation of the nanoparticles was examined on antibacterial effect using colonies of *Staphylococcus Aureus* and *Escherichia coli.*

1. Introduction

In recent years with the increasing applications of nanotechnology, is known that nanomaterials like Iron oxide (Fe_3O_4), Titanium oxide (TiO_2) and Zinc oxide (ZnO) have shown great properties for applications in heavy metals removal from polluted water, industry wastewater treatment, biomedicine and photocatalysts [1-7]. This features is due to properties of nanoparticles as nano-adsorbents removing heavy ions and because of its size have ability to interact with light which yields the confinement of light inside the nanoparticles (NPs) which generates new non-linear phenomena such as the collective oscillations of conduction band electrons in spherical metal nanoparticles excited by external electromagnetic field, so-called localized surface plasmon resonance (LSPR), this phenomenon leads to a strong enhancement of the local electromagnetic fields surrounding the NPs at a specific wavelength. LSPR frequency can be tuned by changing the characteristics of the NPs like for example shape, size and liquid environment, this is being widely used for medical applications of biological sensing systems, photovoltaic cells and efficient catalysis processes like plasmonic solar desalination as reported by *Tianyu Liu et.al* [8, 9].

Because the ideal plasmonic photocatalysts should simultaneously act as an absorber to capture light as well as a catalytic surface to interact properly with surface intermediates, metal nanoparticles with strong light absorption capability have been demonstrated as a new family of plasmonic photocatalysts that offer distinctly different benefit compared to conventional semiconductor photocatalysts, as example of this *Jianlong Wang et.al* demonstrate that Fe_3O_4 magnetic nanoparticle can greatly enhance the localized surface plasmon resonance (LSPR) of metal nanoparticle in biological systems, *Nayareth Soltani and Elias Saion* reported degradation of methylene blue by visible light induced in the presence of photocatalytic ZnS and CdS nanoparticles [10-14].

Iron oxide nanoparticles with titanium, zinc couple can be a very promising photocatalytic system for both UV and visible light- induced reactions [15, 16]. Zn and Ti NPs as surface modifiers of Fe_2O_4 can inhibit electron- hole recombination under UV irradiation working as an electron sink, because Fermi energy level of metallic Zn and Ti lies below the conduction band of Fe_2O_4, and therefore photo excited electrons in Fe_2O_4 can be easily transferred the charge to ZnO and TiO_2 NPs [17, 18]. The advantage of functionalized the bimetallic systems with noble metal or semiconductors NPs is that they can activate Fe_2O_4, towards visible light and UV-light due to localized surface plasmon resonance (LSPR) of the noble metal, thus being so-called "plasmonic-photocatalysts" [19 - 21]. The mechanism of plasmonic photocatalysts can be used especially in processes involving chemical transformations for example in degradation process of polluted substances or industrial waste water treatment where is possible used the iron as catalyst and enhancement their plasmonic properties doping with a semiconductor and adding light [20, 22, 23].

Pulsed laser ablation method in liquid environment has been studied as a new alternative to preparation nanoparticles without contamination [24, 25]. Moreover, this technique is being widely studied for the practical design of nanoparticles structure changing the experimental parameters, which is very useful when modifying the plasmonic properties of metal nanoparticles [26, 27]. In this work metal oxide nanoparticles (MONPs) were prepared by laser ablation technique in liquid environment. Optical and plasmonic properties of the colloidal NPs were investigated using UV-Vis absorbance spectroscopy and Fourier transform infrared spectroscopy (FTIR), nanoparticle morphology analysis was done with scanning electron microscopy (SEM). In addition, NPs were studied in microbiological systems by photo activation of NPs and their antibacterial effect front colonies of *S. Aureus* and *E. Coli.*

2. Experimental Details

2.1. Synthesis of metal oxide nanoparticles

Figure 1 shown the schematic optical set-up used for pulsed laser ablation in liquid environment. Deionized water was put in a glass beaker until 4 mm above the surface of the target. The laser beam was focused, with a semi spherical lens onto the surface of a solid rotating target through the liquid transparent. We used a short-pulse, Q-Switched Nd: YAG laser which provided 7 ns, 80 mJ pulses at a wavelength of 1064 nm and 532 nm with repetition rate of 10 Hz and 20 Hz for each wavelength respectively. The fluence was 0.8 J/cm^2 for 1064 nm and 532 nm respectively. The colloidal NPs samples were prepared from $TiFe_2O_4$ and $ZnFe_2O_4$ solid targets, and were ablated during 15 minutes in 6 ml of liquid.

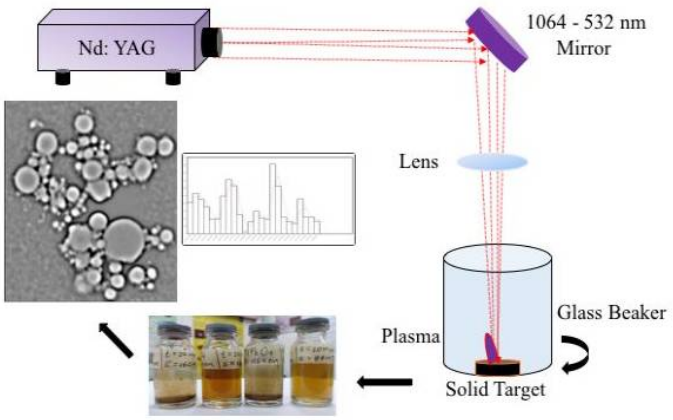

Figure 1. Experimental Set-up used for laser ablation in liquid environment, samples of colloidal NPs and SEM images with size histogram.

2.2. Characterizations of metal oxide nanoparticles

The optical properties of the NPMs synthesized were investigated with UV-Vis spectroscopy using a UV-visible spectrophotometer Evolution 201/220 from the Thermo Scientific series of quartz cuvettes with an optical path of 1 cm. To determine vibration modes of NPs we used infrared spectroscopy by Fourier transform (FTIR), using an Agilent Carry 630 FTIR Infrared spectrometer. The SEM micrographs to study structure and shape were obtained with a Phenom XL electronic scanning microscope in standard mode with an acceleration voltage range between 10 kV and 15 kV.

2.3. Microbiological Experiment

The batch experiments were done by triplicated method, from 1 to 3 isolated colonies of *S. Aureus* and *E. Coli* were taken in selective media, such as; Baird Parker Agar and EMB Agar (Eosin and Methylene Blue), then transferred to 9 mL of IBH broth (Infusion-brain-heart) and incubated at 37 ° C, with shaking, making dilutions until reaching an optical density at 540 nm between 0.4 and 0.6 using the McFarland standard method, corresponding to the exponential phase of growth. Subsequently, 100 µL of the inoculum was taken and transferred to a Petri dish, containing 20 mL of IBH agar (Infusion-brain-heart), incubated at 37 ° C, after agitation to homogenize the growth of microorganisms in the media.

3. Results and Discussion

3.1. UV-Vis Analysis

MONPs exhibit surface plasmon resonance peak in 300 nm and 271 nm for $TiFe_2O_4$ and $ZnFe_2O_4$ respectively produced with wavelength of 1604 nm (figure 2a). Whereas that for 532 nm of wavelength MONPs produced with 532 nm no peak is observed (figure 2b). The absorption spectra of $TiFe_2O_4$ and $ZnFe_2O_4$ nanoparticles is shown in Figure 2. These spectra reveal that maximum value appears in UV region, which is characteristic absorption edge of this type of ferrite NPs. In addition, the sharp peak indicates formation of stable colloidal suspension [28]. The difference between figure a) and b) indicates a change in concentration as in the nanostructure of nanoparticles. On the other hand, the noise that presents the spectra at 1064 nm indicates a higher production of nanoparticles than for those prepared with wavelength of 532 nm.

The bands around 210 and 270 nm in figure 2a are attributed to the charge transfer bands that have the Fe^{+3} of the iron ions isolated in tetrahedral (Td) and octahedral (Oh) coordination, respectively [29]. The peak of around 330 nm is assigned to Fe^{3+} isolated in any of the ulvoespinelas [30, 31]. In addition, the absorption region between 200 and 300 nm in figure 2b) could also be assigned to the charge transfer between the oxygen ions and the Fe^{+3} ions [32]. In this range, there is a superposition with the iron and oxygen charge transfer bands. In the analysis carried out by UV-vis-DRS, it suggests the presence of the ulvoespinelas of MFe_2O_4, where M is Ti^{+2} or Zn^{+2}, respectively, which are present as nanoparticles in two structures in tetrahedral coordination (Td) and M in octahedral (Oh), respectively.

The figure 2c and 2d show the spectra of colloidal MNPs a month afterwards of synthesis for 1064 nm and 532 nm. For NPs prepared with wavelength of 532 nm, a peak around 350 nm appear, evidencing agglomeration and formation of larger particles, this is according to theory corresponding with LSPR [33-35]. Whereas in MONPs produced with wavelength of 1064 nm change is observed. For both samples a new peak with lower intensity is observed around 970 nm, which corresponds to new modes of oscillation of the agglomerated nanoparticle. This results shown enhancement of the LSPR effect, since the appearance of a new peak in near infrared region would improve the efficiency of this nanomaterial absorbing radiation. The table 1 show the principal parameter measured of the nanoparticle.

From a quantum point of view, a high percentage of atoms is accumulated on NPs surface, exhibiting a special characteristic with light surface interaction like LSPR. These special characteristics are caused by the effects of quantum confinement effect of metallic nanoclusters of $TiFe_2O_4$ and $ZnFe_2O_4$, which cannot be seen in bulk material [25, 36, 37].

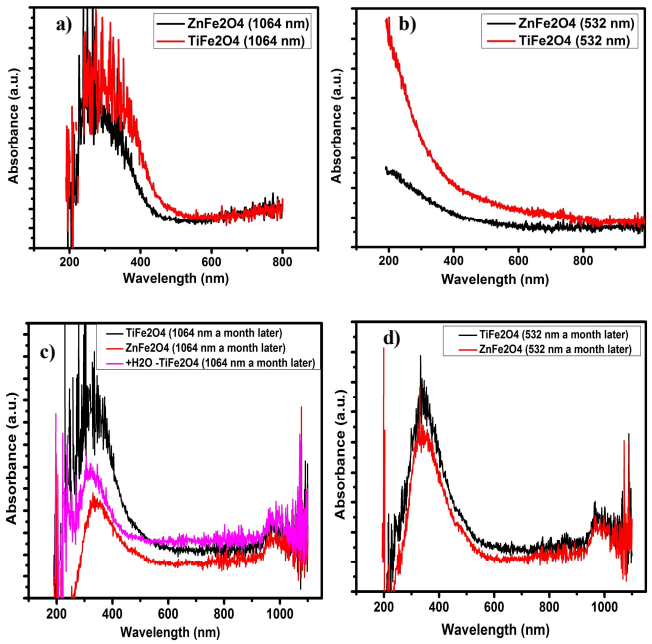

Figure 2. UV-Vis absorbance spectra of MONPs produced with laser ablation technique in water at 1064 and 532 nm of wavelength.

Table 1. Principal Absorbance Peak of MONPs

Metallic Target	1064 nm Peaks Position		532 nm Peaks Position	
	As Growth	1 Month	As Growth	1 Month
$TiFe_2O_4$	300 nm	325 nm 970 nm	210 nm	342 nm 978 nm
$ZnFe_2O_4$	271 nm	343 nm 975 nm	200 nm	346 nm 980 nm

Preprints (www.preprints.org) | NOT PEER-REVIEWED | Posted: 14 January 2019 doi:10.20944/preprints201901.0127.v1

Peer-reviewed version available at Colloids Interfaces 2019, 3, 25; doi:10.3390/colloids3010025

3.2. Band Gap Estimation

The band gap is a key indicator of its light harvesting efficiency under solar illumination. To estimated band gap energy of NPs we used Tauc's relation, equation 1 from UV-Vis absorption spectra for a direct band gap $n = ½$ [38, 39].

$$(\alpha h\nu)^{\frac{1}{n}} \propto (h\nu - E_g) \qquad (1)$$

Band gap energy results for MONPs is shown in table 2. The optical energy for $TiFe_2O_4$ and $ZnFe_2O_4$ changes slightly between 2.17 eV and 2.27 eV, this values are according with reported in previous work showing a magnetic semiconductor behavior [40, 41]. This results have a great variety photocatalysts applications in environmental clean since a small band gap is also important as is reported in previous works [14, 34].

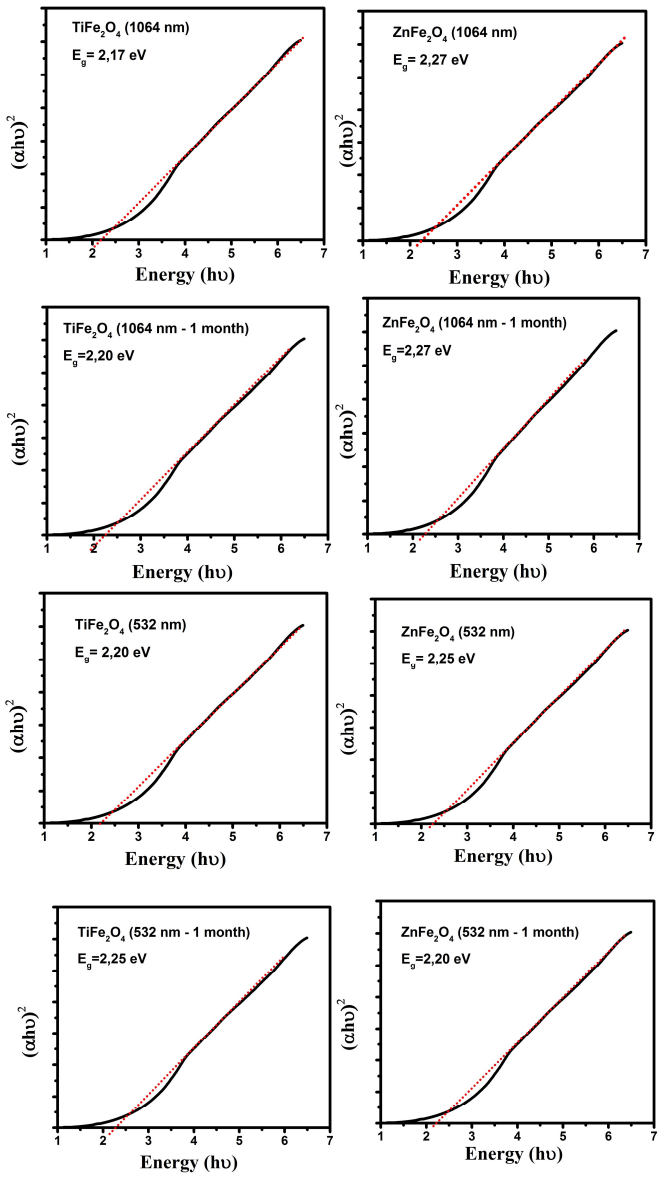

Figure 3. Optical band gap of MONPs produced with laser ablation technique in water at 1064 and 532nm of wavelength.

Table 2. Optical band gap of MONPs produced with laser ablation technique in water at 1064 and 532nm of wavelength.

Target	E_{gap} (eV) at 1064 nm	E_{gap} (eV) at 1064 nm (1 month)	E_{gap} (eV) at 532 nm	E_{gap} (eV) at 532 nm (1 month)
$TiFe_2O_4$	2.17	2.20	2.20	2.25
$ZnFe_2O_4$	2.27	2.27	2.25	2.20

3.2.1. Size determination using band gap energy

Several theoretical models have been proposed in the literature, aiming to give a quantitative agreement of the predicted dependence of energy band gap on the particle size [42, 43]. The commonly used one is the Brus model, described by equation 2.

$$\Delta E = E_{nano} - E_{bulk} = \frac{h^2\pi^2}{2M_{ef}R^2} \qquad 2)$$

where E_{bulk} is band gap of the bulk material, E_{nano} is band gap of nano material, h is Planck's constant, R is the radius of the particles and M_{ef} is the effective mass of the system. According to equation 2 the nanoparticles size estimated was between 4.69 nm and 4.76 nm. The results are presented in table 3.

3.3. FTIR- Analysis

FTIR spectra of colloidal NPS are shown in figure 4. An intense characteristic absorption band between 3300 cm^{-1} and 3500 cm^{-1} assigned to the fundamental mode of vibration to O-H stretching and deformation, due to water absorption, on the metal Surface. Moreover, appear a bands in 1637 cm^{-1} and 2100 cm^{-1} attributed to scissor bending vibration of molecular water. Vibrational peaks around 415 cm^{-1} reveal mainly Fe–O stretching vibration bonds. Appearance of peaks around 1600 cm−1 correspond to the overlapping of Ti–O, Fe–O–Ti, Zn–O, Fe–O–Zn bonds of ferrite nanoparticles. All samples synthetized exhibit similar FTIR spectra, this results indicated that the structure of the MONPs is not altered by infrared radiation, regardless of the wavelength of synthesis [33, 37].

Table 3. Size estimation of MONPs produced with laser ablation technique using band gap energy results.

Target	Size(nm) (1064 nm)	Size (nm) (1064 nm 1 month)	Size(nm) (532 nm)	Size(nm) (532 nm 1 month)
$ZnFe_2O_4$	4.70	4.68	4.75	4.70
$TiFe_2O_4$	4.69	4.69	4.72	4.75

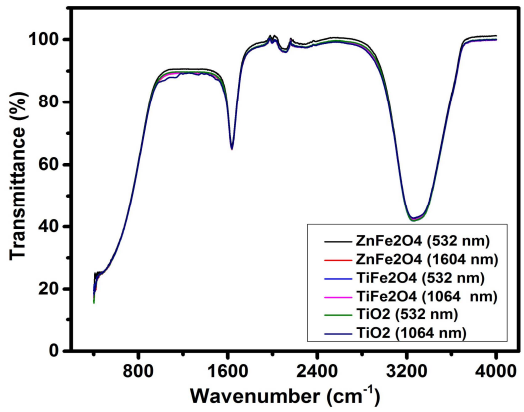

Figure 4. FTIR transmittance spectra of MONPs produced with laser ablation technique in water at 1064 and 532nm of wavelength.

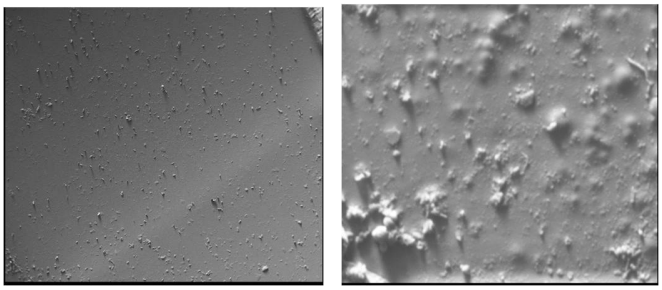

Figure 5. SEM images of MONPs.

3.4. Scanning Electron Microscopy

From SEM micrographs we observed that particles are spherical in shape and have a polidispersive particles size. In figure 5 left side is shown the SEM image of $TiFe_2O_4$ these nanoparticles have a homogenous morphological distribution over substrates of silica, while $ZnFe_2O_4$ figure 5 right side have tendency to form bigger clusters which indicated that $ZnFe_2O_4$ was instable with precipitation in the colloid before the deposition on the substrate. Furthermore, this results show that Ti and Zn is incorporated with Fe to form spherical like structures typically of the metal nanoparticles prepared by laser ablation method [26, 27]. In addition, after one month, all samples exhibit agglomeration due to highly magnetic behavior of titanium and zinc ferrite NPs as well as is reported in literature [28, 33].

4. Application as antibacterial surfaces

The sensitivity of strains of *S. Aureus* and *E. Coli* were determined using the method of planting by depth according to the Institute of Clinical and Laboratory Standards (CLSI, 2015). Seeding was performed in triplicate in each programmed experiment, with two incubation periods of 24 and 48 hours at 37ºC, modifying their exposure to visible light and UV light for 2 hours in some cases. The antibiotic used as a positive control was reactive grade ampicillin, with a concentration of 1000 ppm and DMSO as target at 5%. Three squares of residual polyethylene with area of 0.25 cm^2 were placed in triplicate, with the nanoparticles deposited which were labeled as follows: A (TiFeO2-1064 nm 100 mJ), B (TiFeO2- 1064 nm- 80 mJ), C (ZnFeO4-1064 nm, 80 mJ), D (TiFeO2, 532 nm, 80 mJ)), E (ZnFeO2, 1064 nm, 84 mJ), F (ZnFeO2, 532 nm, 80 mJ), this can be seen in figure 7. Subsequently, all samples were exposed to UV radiation at 330 nm, for a time of 2 hours; comparing the antibacterial activity in the absence of light the NPs show enhancement of antibacterial activity when them were illuminated with UV light, which indicated the photo activation of their plasma oscillation at surface of the NP such that it interacts strongly with the bacteria preventing its spread. For the interpretation of the results, the strains were classified as susceptible, intermediate or resistant with respect to the evaluated nanoparticles, measuring the inhibition halo (CLSI, 2015) this results are deposited in table 4 [44-48]. In this experiments nanoparticles of $TiFe_2O_4$ prepared at 532 nm shown the better anti-bacterial results exhibiting an inhibitions ring of the 30 mm of diameter in samples deposited in polyethylene substrates when this was illuminated with UV light at 330 nm.

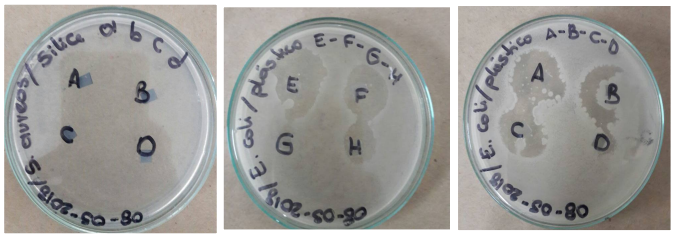

Figure 7. MONPs and antibacterial activity in colonies of *Eschericia coli*.

Table 4. Measurements of the inhibition ring according to (CLSI, 2015).

NPs	*Illuminated at 330 nm [hours]*				*Without light [hours]*			
	S. Aureus		*E. coli*		*S. Aureus*		*E. coli*	
Incubation time at 37°C	**24**	**48**	**24**	**48**	**24**	**48**	**24**	**48**
$TiFeO_4$, 1064 nm	23 mm ±0.1 **S**	24 mm ±0.1 **S**	23 mm ±0.1 **S**	24 mm ±0.1 **S**	**R**	**R**	**R**	**R**
$TiFeO_4$, 532 nm	30 mm ±0.3 **(S)**	30 mm ±0.1 **(S)**	28 mm ±0.3 **(S)**	29 mm ±0.3 **(S)**	**R**	**R**	**R**	**R**
$ZnFeO_4$, 1064 nm	17 mm ±0.1 **(I)**	18 mm ±0.2 **(I)**	9.7 mm ±0.2 **(R)**	10 mm ±0.3 **(R)**	**R**	**R**	**R**	**R**
$ZnFeO_4$, 532 nm	19 mm ±0.3 **(I)**	19 mm ±0.1 **(I)**	20 mm ±0.1 **(S)**	21 mm ±0.2 **(S)**	**R**	**R**	**R**	**R**
Polyethylene	R	R	R	**R**	**R**	**R**	**R**	**R**
Positive control (ampicillin)	23 mm	23 mm	23 mm	23 mm	23 mm	23 mm	23 mm	23 mm

S (Sensitive, ≥20 mm), **I** (Intermediate, 15-20 mm), **R** (Resistant, ≤14), (CLSI, 2015).

5. Conclusions

In summary metal oxide nanoparticles were prepared by laser ablation technique, this MONPs have spherical forms with different size and shown the same color aspect, the $TiFe_2O_4$, NPs were most stable that $ZnFe_2O_4$ due to that the last present fast agglomeration. The Plasmon resonance peak appears around 300 nm, 274 nm for $TiFe_2O_4$, and $ZnFe_2O_4$ respectively, produced at 1604 nm, unlike the nanoparticles produced at 532 nm we not observe the formation of a peak. The maximum absorbance of radiation in the UV range between 200 nm and 350 nm, indicate the favorability of this NPs for applications in catalysts, photocatalysts and surface process. However, for both samples we found that the maximal absorbance of radiation is in the UV range, a month later we found that the NPs present a new absorption band in the infrared range with low intensity which is a good indicator of nanostructure modification. The optical properties of the colloidal nanoparticles depended of the laser wavelength which is manifested in the variation of UV- Vis spectra and band gap energy. In batch experiments the $TiFe_2O_4$, nanoparticles prepared at 532 nm shown the better anti-bacterial results exhibiting an inhibitions ring of the 30 mm of diameter in samples deposited in polyethylene substrates when this was illuminated with UV light at 330 nm.

Acknowledgments

We acknowledge the financial support provided by Colciencias & Vicerrectoria de Investigaciones Innovacion y Extension Universidad Tecnológica de Pereira (Convocatoria 775 Jovenes Investigadores por la paz 2017 codígo de proyecto JI3-18-1 y Proyecto 3-18-7.)

6. References

[1] Afshar et al. Pollution, 3(3): (2017), 505-516. DOI: 10.7508/pj.2017.03.014
[2] I. C. Nica, *et al.* Int. J. Mol. Sci. (2017), Vol 18, 249. doi:10.3390/ijms18020249.
[3] Wan Yaacob W.Z *et al.* Chemical Engineering Transactions. Vol 28-2012, 25-30.
[4] P. N. Dave *et al*. Journal of Nanotechnology Vol 2014, Article ID 398569. http://dx.doi.org/10.1155/2014/398569.
[5] Y.C. Sharma et al. Environmental Technology. Vol. 30, No. 6, May 2009, 583–609.
[6] Z. Rafiq *et al*. Journal of Environmental Chemical Engineering 2 (2014) 642–651.
[7] C. Berndt *et al* Mat. Res. Soc. Proc.Volume 740, I15.4 (2003).
[8] Tianyu Liu *et al*. Nature Photonics 10, 361–362 (2016).
[9] T. R. Jensen *et al*. J. Phys. Chem.B,104(45), 10549–10556 (2000).
[10] Katherine A. *et. al.* Annu. Rev. Phys. Chem. 2007. 58:267–97.
[11] Wang, Jianlong *et. al* . *Anal. Chem.*, 2010, *82* (16), pp 6782–6789.
[12] Murph S.E, *et al*. J. Vis. Exp. (108), e53598, doi:10.3791/53598 (2016). https://www.jove.com/video/53598.
[13] Mi Jung *et al.* Opt. Eng. 55 (8), 087107 (2016), doi: 10.1117/1.OE.55.8.087107.
[14] N. Soltani *et. al.* Int. J. Mol.Sci.2012,13,12242-12258; doi:10.3390/ijms131012242.
[15] E. Kowalska *et al.* Catalysts 2017, 7, 317; doi:10.3390/catal7110317.
[16] Zaizhu Lou. *et al.* Chem.Cat.Chem, 00, 1–22. (2014).
[17] H. Ghaforyan *et.al* World appl. programming, Vol (5), No (4), April, 2015. pp. 79-82
[18] K.L. Kelly *et.al*. *J. Phys. Chem. B*, 2003, *107* (3), pp 668–677
[19] W. Hergert. *et. al.* The Mie Theory, Springer Series in Optical Sciences 169, Springer-Verlag Berlin Heidelberg 2012. DOI: 10.1007/978-3-642-28738-1_2
[20] Xuming Zhang *et al* 2013 *Rep. Prog. Phys.* 76 046401.
[21] Y. D. Chiou. *et. al.* Appl. Catal. B., 2011, 105, 211.
[22] S. Li et al. / Journal of Hazardous Materials 322 (2017) 163–171. http://dx.doi.org/10.1016/j.jhazmat.2016.01.032.
[23] U.A. Agú, *et al*., Journal of Magnetism and Magnetic Materials (2014), http://dx.doi.org/10.1016/j. jmmm.2014.06.046i
[24] M. Boutinguiza, *et al*. Applied Surface Science 258 (2012) 9484–9486. http://dx.doi.org/10.1016/j.apsusc.2012.05.148.
[25] A. Hamad *et al.* Appl. Phys. A (2016), 122;904.
[26] F. Bozon *et al*. Quantum Electronics (2003), 33(8), 714-720.
[27] Fojtik. *et al.* Phys. Chem. 1993, 97(2), 252–254.
[28] A. Shukla *et al* Adv. Mater. Lett. 2015,6 (12), 1066-1072
[29] T. Kawabata et al. J. Mol. Catal. A: Chem. 253 (2006) 279–289.
[30] Y. Ohishi et al. Appl. Catal., A 288 (2005) 220-223.
[31] A. Heredia, et al. J. Magn. Magn. Mater. 234 (2013) 38-46.
[32] Verónica R, et al.Top. Catal 54 (2011) 277–286.
[33] J. Ho Ryu *et al*. / Journal of Luminescence 124 (2007) 67–70.
[34] A. Shukla *et al.* J Mater Sci: Mater Electron, DOI 10.1007/s10854-017-7423-3.
[35] J.S. Duque *et al* 2017 J. Phys: Conf. Ser. 850 012017.
[36] Gupta S M, *et al*. Chinese Sci Bull, 2011, 56: 1639−1657, doi: 10.1007/s11434-011-4476-1.
[37] Akimoto. S. *et al* (1957). Journal of Geomagnetism and Geoelectricity, 9(4), 165–178. doi:10.5636/jgg.9.165
[38] Tauc *et al.* Phys. Stat. Sol. 15, 627 (1966).
[39] N. Ghobadi. International Nano Letters, 3:2, 2013, doi: 10.1186/2228-5326-3-2
[40] K. Kirchberg, *et al* J. Phys. Chem. C 2017, 121, 27126−27138. DOI: 10.1021/acs.jpcc.7b08780.
[41] Song Sun. *et al* (2012) Progress in Natural Science Vol 22, 6 pages 639-643. https://doi.org/10.1016/j.pnsc.2012.11.008
[42] T. Theivasanthi *et. al* Research and Application of Material (2013) 36-43.
[43] S. Baset. *et. al.* Journal of Nanomaterials and Biostructures. Vol. 6, No 2, 2011, p. 709 – 716.
[44] S.K. Bajpai *et al.* / Carbohydrate Polymers 153 (2016) 60–65.
[45] H.E. Ghandoor, *et al*. Int. J. Electrochem. Sci., Vol. 7, 2012
[46] D. H. Taffa, *et al* J. Photon. Energy 7(1), 012009 (2016), doi: 10.1117/1.JPE.7.012009.
[47] Novel Stabilization Mechanism on Polar Surfaces: ZnO (0001)-Zn, Phys. Rev. Lett. 90, 016102 – Published 8 January 2003.
[48] V.C. Ferreira *et al.* Journal of Photochemistry and Photobiology A: Chemistry 357 (2018) 201–212.